JOURNAL OF MATERIALS SCIENCE **34** (1999) 6035–6040

Characterization of borophosphosilicate glass soot fabricated by flame hydrolysis deposition for silica-on-silicon device applications

CHOON-GI CHOI,* MYUNG-YUNG JEONG, TAE-GOO CHOY
Component Technology Development Department, Electronics and Telecommunications Research Institute, Taejon, 305-350, Republic of Korea
E-mail: cgchoi@etri.re.kr

The use of flame hydrolysis deposition (FHD) to fabricate porous silica glass soot in the B_2O_3-P_2O_5-SiO_2 glass system (BPSG) is described for silica-on-silicon device applications. The deposition conditions with a Si substrate temperature (∼200 °C) and a flame temperature (1300–1500 °C) are appropriate to synthesize the SiO_2 and P_2O_5-SiO_2 non-crystalline glass soot. However, further investigations for the B_2O_3-P_2O_5-SiO_2 glass soot are needed to obtain complete amorphous phases. The densification process of porous silica glass soot in the three systems of SiO_2, P_2O_5-SiO_2 and B_2O_3-P_2O_5-SiO_2 is also described to estimate the onset of sintering temperature. The OH absorption measurements are performed to try to identify incorporation of hydroxyl contaminants in the systems of P_2O_5-SiO_2 and B_2O_3-P_2O_5-SiO_2. © *1999 Kluwer Academic Publishers*

1. Introduction

Silica glass soot (fine glass particles) are very important in the fabrication of silica-based planar lightwave circuits on silicon [1]. The material properties of glass soot are governed by the characteristics of its constituent materials and the deposition conditions. They possess the properties of the final silica glass films. The influence of the deposition conditions is direct on the structural characteristics of the silica glass soot. Several authors [2–9] have investigated the structural properties of silica glass soot.

Borophosphosilicate glasses (BPSG) are generally used in the areas such as optical fiber preform, VLSI (very large scale integration), and silica-on-silicon device. BPSG glasses are fabricated by several methods such as CVD (chemical vapor deposition), sol-gel, and FHD (flame hydrolysis deposition). CVD methods for deposition of BPSG for low temperature core reflow in VLSI fabrications were developed at RCA [10–12]. Methods of this type are now used for silica-on-silicon device fabrication by AT&T [13]. Becker *et al.* [14] at Siemans AG were also used CVD method for deposition of tetraethylorthosilicate-borophosphosilicate glasses in megabit DRAM device fabrications. Kern and Smeltzer [12] reported that B_2O_3 reduces the temperature of viscous deformation when added to PSG, and in effect allows a desirable lowering of the phosphorus concentration in the glass to attain fusion at a given temperature. Different routes to the synthesis of borophosphosilicate glass by sol-gel process have been described by several authors [15–17]. They used boric and phosphorous oxides, boric and phosphoric acids, and boron triisopropoxide and triethyl-phosphate as sources for B_2O_3 and P_2O_5, respectively. The development of low temperature processes for fabrication of low-loss, OH-free BPSG silica-on-silicon devices by sol-gel method are described by Syms *et al.* [18, 19]. They explained that the viscosity of phosphosilicate (PSG) depends on the P_2O_5 concentration and both B_2O_3 and P_2O_5 increase the thermal expansion coefficient of SiO_2, reducing the stress caused by thermal mismatch with the Si substrate. FHD, which is first developed at NTT [20], allows the fabrication process to proceed vertically, as a cladding substrate can be fabricated on which a second layer is deposited, without adversely affecting the underlying structure. The NTT achievements on high silica content glass technology and its application to integrated-optic components are reported by Kawachi [1]. The use of B_2O_3 and P_2O_5 to lower the sintering temperature of glasses deposited by FHD for silica-on-silicon device applications to allow waveguided core reflow are first described by Sun *et al.* [21]. The FHD process has the advantage of being able to fabricate thick layers up to ∼100 μm at high deposition rates (∼1 μm/min). Moreover, glass deposition is relatively easy except for a wafer bowing, which results from one-sided deposition [22].

In the present paper, the use of FHD to fabricate porous silica glass soot in the B_2O_3-P_2O_5-SiO_2 glass system (BPSG) is described. BPSG glasses were used to fabricate buffer and cladding layers for silica-on-silicon device fabrication. For that purpose, porous

* Author to whom all correspondence should be addressed.

silica glass soot in the three systems of SiO_2, P_2O_5-SiO_2 and B_2O_3-P_2O_5-SiO_2 are characterized by using a scanning electron microscopy (SEM), X-ray diffractometry (XRD), thermogravimetric analysis (TGA), differential scanning calorimetry (DSC), fourier transform infrared spectroscopy (FTIR), and electron probe microanalysis (EPMA). The structural properties, dopant-dependent densification processes, dopant contents, and absorption characteristics have been studied.

2. Experimental

2.1. Formation of silica glass soot

Silica glass soot synthesized with a FHD setup is deposited directly on Si wafers (100) placed X-Y movable stages, which are kept at about 200 °C. A mixture of raw gaseous metal chloride materials, such as $SiCl_4$, $POCl_3$, and BCl_3, is hydrolyzed into metal oxides in an oxy-hydrogen torch flame. The flame torch is placed perpendicular to samples. The chlorides are vaporized in carrier gases, such as O_2 and He, with the bubbling technique, and mass flow controllers (MFC) control flows of the carrier gas through the bubblers. Transferred submicron metal oxide particles are nucleated by the hydrolysis reaction, cohered by the Brownian motion, and then synthesized in polydisperse particles. These particles are deposited by the thermophoretic mechanism. At the high temperature flame (1300–1500 °C) provided by a mixture of O_2 and H_2 gases, the input $SiCl_4$ and dopants react rapidly and completely. The process of silica glass soot formation can be described by the following oxidation and hydrolysis reactions:

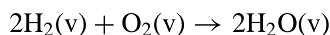

$$2H_2(v) + O_2(v) \rightarrow 2H_2O(v)$$

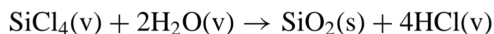

$$SiCl_4(v) + 2H_2O(v) \rightarrow SiO_2(s) + 4HCl(v)$$

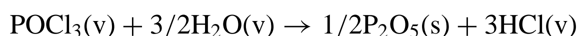

$$POCl_3(v) + 3/2H_2O(v) \rightarrow 1/2P_2O_5(s) + 3HCl(v)$$

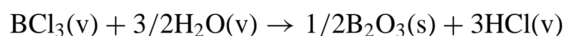

$$BCl_3(v) + 3/2H_2O(v) \rightarrow 1/2B_2O_3(s) + 3HCl(v)$$

where v is vapor and s is solid.

2.2. Measurement on glass particles

The silica glass fine particles were analyzed by using SEM, XRD, TGA-DSC, FTIR, and EPMA. The morphology of glass particles was observed by SEM after gold coating. XRD measurements (CuK_α radiation) were used to identify crystalline or non-crystalline states of glass particles. Powder samples were used to avoid peak interferences between samples and Si wafer. The radiation of $\theta/2\theta$ scanning was performed in angle range between $2\theta = 10°$ and $2\theta = 80°$ with a scanning speed of 4°/min and a power of 40 kV and 45 mA. TGA and DSC measurements were performed to determine changes in sample weight and to study the thermal behavior undergoing physical and chemical changes during the heat treatment. Samples with a weight of about 15 mg were charged in Pt crucibles and then heated for a temperature range from room temperature to 1300 °C at a heating rate of 40 °C/min in air. FTIR was used to study the molecular level structure of glass particles prepared by the FHD. The glass particles were compressed into a thin pellet with KBr, which is transparent in the IR. The composition of transparent BPSG buffer and cladding layers in the ternary system were analyzed by EPMA.

3. Results and discussion

Fig. 1 shows typical SEM micrographs of SiO_2, P_2O_5-SiO_2 and B_2O_3-P_2O_5-SiO_2 glass particles deposited on the Si substrates. The glass soot is formed by uniform spherical particles with a diameter estimated to be 0.01–0.1 μm in the three systems. The appearances of the SiO_2, P_2O_5-SiO_2 and B_2O_3-P_2O_5-SiO_2 glass particles are very similar to each other, and show very porous structures. These particles tend to form large agglomerates that result in forming bodies with low bulk densities, and, consequently, follow large shrinkages during sintering. The average pore size is several times larger than the average particle size [3].

Fig. 2 shows the spectra of XRD measurements for the three systems of SiO_2, P_2O_5-SiO_2 and B_2O_3-P_2O_5-SiO_2 glass particles. Spectrum a) represents that SiO_2 particles prepared from a flame hydrolysis reaction is completely amorphous state. SiO_2 particles prepared from $SiCl_4$ are always formed in the non- crystalline state, irrespective of the reaction conditions [5]. This spectrum is composed of a broad diffraction peak at $2\theta = 21°$, which is attributed to the amorphous glass state of SiO_2.

In the case of P_2O_5-SiO_2 particles, these particles are deposited on Si wafers whose temperature is kept at about 150 °C. The XRD spectrum shows a broad diffraction peak whose appearance is exactly similar to the case of SiO_2 particles. From this result, we can make an assumption that the P_2O_5 particles are also formed in the amorphous state and have no effect on the XRD pattern. The non-crystalline state of P_2O_5-SiO_2 particles is observed in the Si substrate temperature range up to 500 °C.

For the ternary B_2O_3-P_2O_5-SiO_2 glass particles, the pattern shown in Fig. 2c shows several sharp diffraction peaks corresponding to the cubic crystalline states of B_2O_3 and the tetragonal crystalline states of BPO_4. The crystalline peaks of the numbers 1, 3, and 4, correspond the (111), (310) and (420) planes of the B_2O_3 cubic system, respectively, and the peak of number 2 is estimated to be originated from the (101) plane of BPO_4 tetragonal system. Woignier *et al.* [23] also observed this borophosphate (BPO_4) crystalline phase from the monolithic mixed aerogels prepared by hydrolysis and polydensation of metalorganic compounds. This phase is very stable in the glass containing simultaneously P_2O_5 and B_2O_3 [23], and cannot be eliminated after heat treatment at 1100 °C. In our previous investigation [24], however, no BPO_4 crystalline phases were observed even at 950 °C. It should be ascribed that this phenomenon has resulted from different raw materials. Edahiro *et al.* [25] reported that the crystalline phase of B_2O_3 at $2\theta = 28°$ was eliminated at substrate temperature of above 450 °C. The crystalline phase of B_2O_3 in the B_2O_3-P_2O_5-SiO_2 system probably includes

(a)

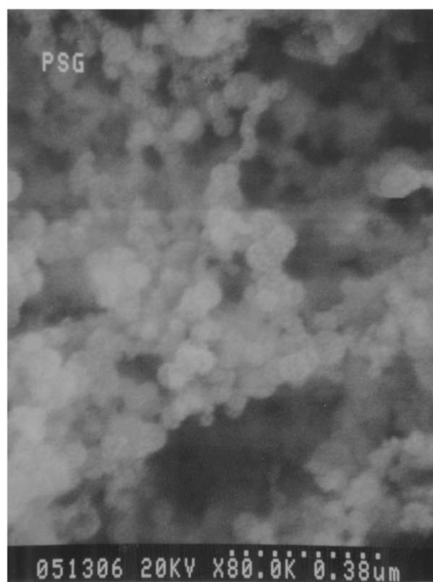

(b)

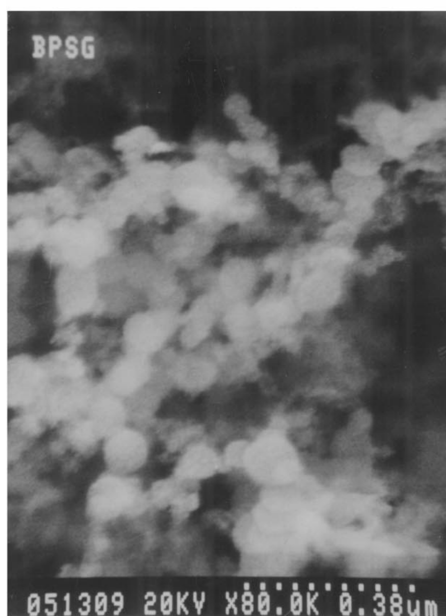

(c)

Figure 1 SEM micrographs of (a) SiO_2, (b) P_2O_5-SiO_2 and (c) B_2O_3-P_2O_5-SiO_2 glass particles.

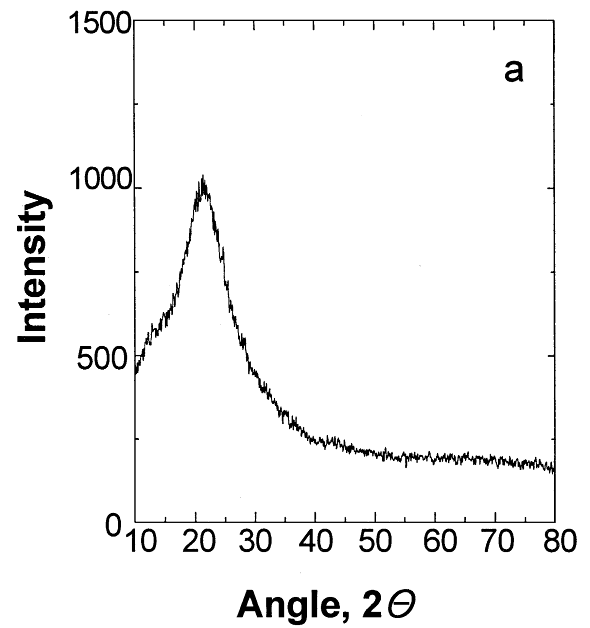

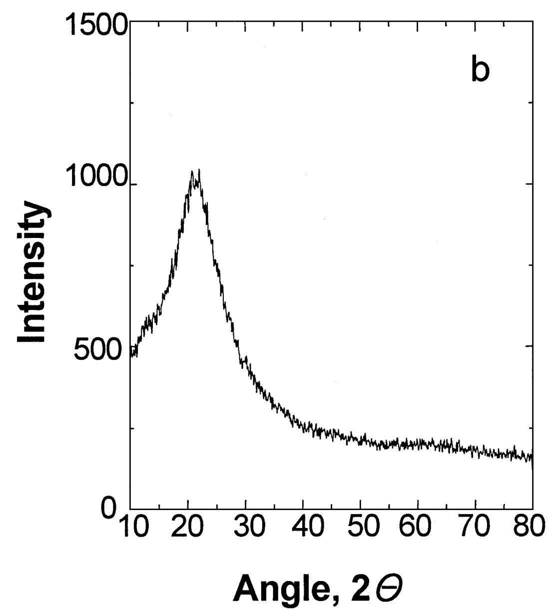

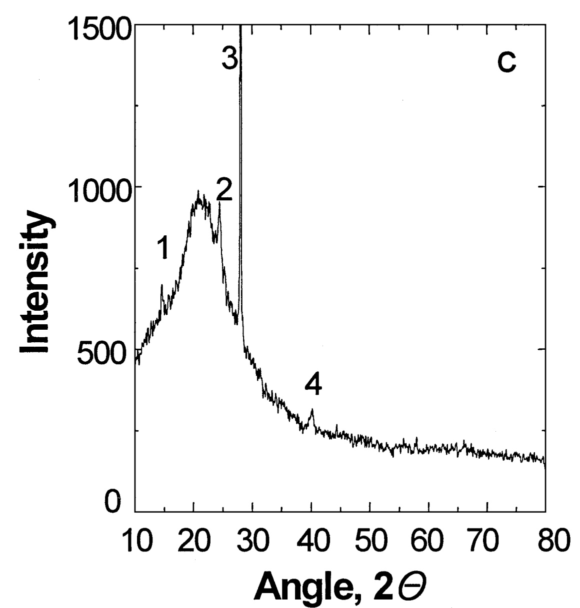

Figure 2 XRD patterns obtained from (a) SiO_2, (b) P_2O_5-SiO_2, and (c) B_2O_3-P_2O_5-SiO_2 glass particles; in the B_2O_3-P_2O_5-SiO_2 XRD pattern (c), 1. B_2O_3 (111), 2. BPO_4 (101), 3. B_2O_3 (310), 4. B_2O_3 (420).

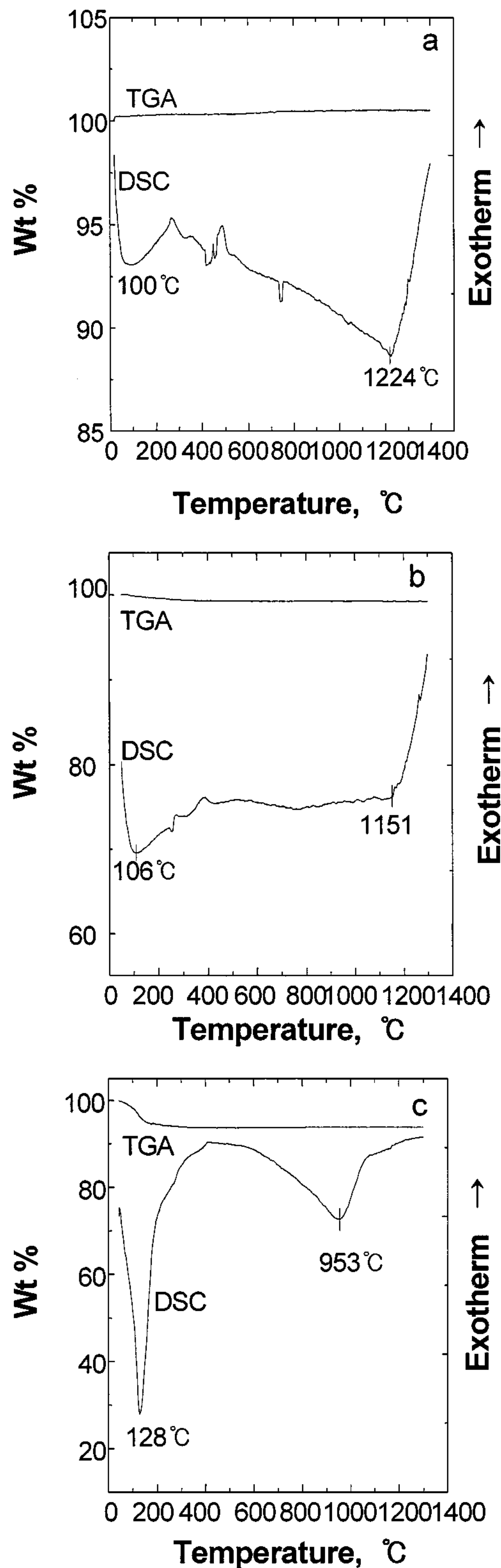

Figure 3 TGA-DSC curves obtained from (a) SiO_2, (b) P_2O_5-SiO_2, and (c) B_2O_3-P_2O_5-SiO_2 glass particles.

a certain quantity of amorphous particles and the degree of crystallinity depends on the soot density [3].

Typical TGA-DSC curves obtained from the SiO_2, P_2O_5-SiO_2 and B_2O_3-P_2O_5-SiO_2 glass particles are represented in Fig. 3. For the SiO_2 glass particles, in the TGA curve, no weight loss is observed as a function of temperature change. This phenomenon indicates that no chemical reactions, such as dehydration, occur during heating [2]. In the DSC curve, a significant baseline change (usually endothermic reaction) occurs below 100 °C. It is based on differences in the heat capacity of the sample and reference. A broad endothermic peak is seen in the temperature range from 270 to 1224 °C. The DSC curve turns abruptly upward at 1224 °C, and finally recovers its baseline. At this turning point of reaction, the SiO_2 particles begin to be densified.

TABLE I Molecular diffusion coefficients in silica glass

Molecule	Diameter (Å)	Diffusion coefficient ($cm^2\ s^{-1}$) 25 °C	1000 °C
Helium	2.0	2.4×10^{-8}	5.5×10^{-5}
Neon	2.4	5×10^{-12}	2.5×10^{-6}
Hydrogen	2.5	2.2×10^{-11}	7.3×10^{-6}
Argon	3.2	—	1.4×10^{-9}
Oxygen	3.2	—	6.6×10^{-9}
Water	3.3	—	$\sim 3 \times 10^{-7}$

The chemical durability of glasses is related to the rate of attack of water and aqueous solutions on glass. This rate is directly related to the solubility of the silica. As the molecules become larger, the molecular solubility becomes smaller, and the diffusion coefficients decrease. Small molecules diffuse rapidly through the silica lattice. The molecular diffusion coefficients in silica glass are compared in Table I [26]. For water molecules, water reacts with the silica lattice as H_2O + Si—O—Si = SiOH—HOSi, and the reacted OH groups have a higher concentration in the glass than dissolved molecular water, so this reaction has a strong influence on the apparent diffusion of water in silica [27]. However, no water diffuse during consolidation, resulting in a small OH absorption in the transparent glass layer because the water molecules have already reacted with glass layer before consolidation.

For the P_2O_5-SiO_2 glass particles, the TGA curve exhibits a very little weight loss. It is known that the moisture-sensitive dopants, such as P_2O_5 and B_2O_3, in the as-deposited glass particles absorb water, but the glass particles existing in the non-crystalline state seem not to be sensitive to water molecules. In the DSC curve, a significant baseline change similar to that of the SiO_2 particles is also observed below 100 °C. A broad peak is also seen in the temperature range from 400 to 1151 °C. The curve turns upward at 1151 °C, and finally recovers its baseline. This peak temperature seems to correspond to the beginning of densification process. As shown in the DSC curve of Fig. 3b, the beginning temperature (1151 °C) of densification process for the P_2O_5-doped glass particles is low in comparison with that (1224 °C) for SiO_2 glass particles.

For the B_2O_3-P_2O_5-SiO_2 glass particles, in the DSC curve, a sharp endothermic peak is observed at 128 °C with a weight loss of about 6% in the TGA curve. This phenomenon seems to result from the water molecule release, and is accelerated in the case of the particles containing the crystalline phases. A broad endothermic peak is observed in the temperature range from 400 to 950 °C, without any weight loss. This peak finally begins to recover its baseline at 953 °C. This point is equal to the temperature at which the densification

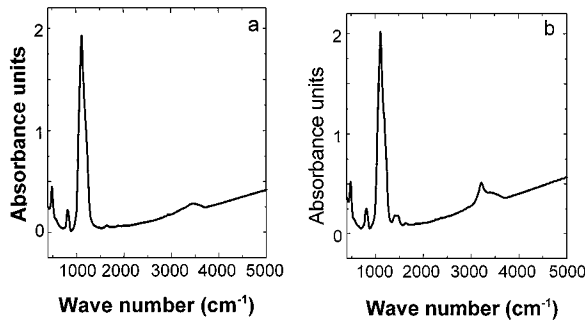

Figure 4 Infrared absorption spectra of (a) P_2O_5-SiO_2 and (b) B_2O_3-P_2O_5-SiO_2 glass particles.

begins. The dopants B_2O_3 decrease again the beginning temperature of densification process.

The same BPSG glass soot was used as buffer and cladding layers. After deposition, the Silicon wafers with BPSG glass soot were introduced into an electric tube furnace for consolidation. The BPSG buffer glass soot was completely densified for 2 h at 1300 °C and BPSG cladding glass soot for 2 h at 1180 °C. The dopant contents of B_2O_3 and P_2O_5 were found to be 2.5 and 2.5 wt % for transparent buffer glass layer and 5.0 and 3.5 wt % for transparent cladding glass layer, respectively. The dopant contents of cladding layer must be higher than those of buffer layer in order to reduce the sintering temperature. The refractive indexes for buffer and cladding layers were calculated from prism coupling measurements and were found to be 1.4480 and 1.4476 at $\lambda = 1.55\ \mu$m, respectively. The calculated error is of the order of 10^{-4}, a value within the accuracy of the measurement setup.

The infrared absorption spectra of the P_2O_5-SiO_2 and B_2O_3-P_2O_5-SiO_2 glass particles were measured, and typical results are shown in Fig. 4. For P_2O_5-SiO_2 (spectrum a), three absorption peaks are observed at 480, 810 and 1110 cm^{-1} for the Si—O—Si bonds. The peak at 480 cm^{-1} is due to bending motions of oxygen atoms perpendicular to the Si—O—Si plane, the peak at 810 cm^{-1} attributed to symmetric stretching motions of oxygen atoms along the bisector of the Si—O—Si bridging angle, and the peak at 1120 cm^{-1} due to asymmetric stretching of oxygen atoms along a direction parallel to Si—Si [8, 28]. The absorption peak near 1210 cm^{-1}, which is not clearly separated, is attributed to fundamental vibrational absorption band of P—O. The small absorption peak observed at 1640 cm^{-1} is probably due to the P—O groups or OH bending mode. The very broad absorption band around 3400 cm^{-1} is resulted from OH impurities. P—OH bonds have a broad vibrational peak at 3300 cm^{-1}, and O—H stretching vibrations induced hydrogen-bonded OH groups and silanol groups (Si—OH) exist in this region [3, 4].

For B_2O_3-P_2O_5-SiO_2 (spectrum b), two different absorption peaks in comparison with P_2O_5-SiO_2 spectrum are observed at 1420 and 3200 cm^{-1}. The absorption peak at 1420 cm^{-1} is attributed to fundamental oscillations of the structural units of B—O. The band at 3200 cm^{-1} is probably due to the B—OH groups, but the fundamental stretching band of B—OH in the glass is 3600 cm^{-1}. Edahiro *et al.* [25] also observed that the absorption peaks at 1450 and 3200 cm^{-1} in the P_2O_5-SiO_2 system. They suggested that the appearance of the 1450 cm^{-1} can be attributed to the existence of H_3BO_3 and that of the 3200 cm^{-1} can be caused by the existence of water impurity combined with B_2O_3 in such a manner as H_3BO_3 and HBO_2. The impurity absorption loss due to hydroxyl (OH^-) groups mainly affects the optical losses in high-silica glasses.

4. Conclusion

The present results and the main conclusions can be summarized as follows:

1) Our deposition conditions with a Si substrate temperature (∼200 °C) and a flame temperature (1300–1500 °C) are appropriate to synthesize the SiO_2 and P_2O_5-SiO_2 non-crystalline glass soot, but the B_2O_3-P_2O_5-SiO_2 glass soot contains the crystalline phases of B_2O_3 and BPO_4. More investigations for the B_2O_3-P_2O_5-SiO_2 glass soot are needed to obtain complete amorphous phases.

2) TGA-DSC measurements are useful to estimate the densification temperature and the effect of dopants. A further reduction in the sintering temperature was achieved by using B_2O_3 in addition to P_2O_5. The densification process has relation to its time, so it is important to find the compromise between a densification temperature and time for the economical densification process.

3) The data on the IR band wavelengths of OH groups are important because they allow for fabricating low loss optical devices. For B_2O_3-P_2O_5-SiO_2, two different absorption peaks in comparison with P_2O_5-SiO_2 spectrum were observed at 1420 and 3200 cm^{-1}. These absorption peaks are due to the B—O band and B—OH groups. A very small quantity of the hydroxyl ions can contribute optical losses in the wavelength regions of commercial interest.

References

1. M. KAWACHI, *Opt. Quant. Electron.* **22** (1990) 391.
2. E. POTKAY, H. R. CLARK, I. P. SMYTH, T. Y. KOMETANI and D. L. WOOD, *J. Lightwave. Tech.* **6**(8) (1988) 1338.
3. M. D. SACKS and T. Y. TSENG, *J. Amer. Ceram. Soc.* **64**(8) (1984) 526.
4. R. M. ALMEIDA and C. G. PANTANO, *J. Appl. Phys.* **68**(8) (1990) 4225.
5. S. TPMARU, M. KAWACHI and T. EDAHIRO, *Jpn. J. Appl. Phys.* **19**(6) (1980) 1197.
6. S. SAKAGUCHI, *J. Non-Cryst. Solids* **171** (1994) 228.
7. *Idem., ibid.* **171** (1994) 249.
8. X. ORIGNAC and R. M. ALMEIDA, *IEE Proc.-Optoelectron.* **143**(5) (1996) 287.
9. O. HUMBACH, H. FABIAN, U. GRZESIK, U. HAKEN and W. HEITMANN, *J. Non-Cryst. Solids* **203** (1996) 19.
10. W. KERN and G. L. SCHNABLE, *RCA Review* **43** (1982) 423.
11. J. E. TONG, K. SCHERTENLEIB and R. A. CAPRIO, *Solid State Technology*, January Issue (1984) 161.
12. W. KERN and R. K. SMELTZER, *ibid.*, June Issue (1985) 171.
13. B. H. VERBEEK, C. H. HENRY, N. A. OLSSON, K. J. ORLOWSKY, R. F. KAZARINOV and B. H. JOHNSON, *IEEE J. Lightwave Tech.* **LT-6** (1988) 1011.

14. F. S. BECKER, D. PAWLIK, H. SCHAFER and G. STAUDIGL, *J. Vac. Sci. Tech.* **B4** (1986) 732.
15. P. N. KUMTA and M. A. SRIRAM, *J. Mater. Sci.* **28** (1993) 1097.
16. K.-S. CHOU, *J. Non-Cryst. Solids* **110** (1989) 122.
17. A. MATSUDA, N. TOHGE and T. MINAMI, *J. Mater. Sci.* **A27** (1992) 4189.
18. R. R. A. SYMS, V. M. SCHNEIDER, W. HUANG and A. S. HOLMES, *Electron Lett.* **31**(21) (1995) 1833.
19. R. R. A. SYMS, W. HUANG and V. M. SCHNEIDER, *ibid.* **32**(13) (1996) 1233.
20. M. KAWACHI, M. YASU and T. EDAHIRO, *ibid.* **19**(15) (1983) 583.
21. C. J. SUN, W. M. MYERS, K. M. SCHMIDT and S. SUMIDA, *IEEE Photon. Tech. Lett.* **3** (1991) 238.
22. M. KAWACHI, *IEE Proc.-Optoelectron.* **143**(5) (1996) 257.
23. T. WOIGNIER, J. PHALIPPOU and J. ZARZYCKI, *J. Non-Cryst. Solids* **63** (1984) 117.
24. C. G. CHOI, M. Y. JEONG and T. G. CHOY, *J. Kor. Ceram. Soc.* **34**(8) (1997) 811.
25. T. EDAHIRO, M. KAWACHI, S. SUDO and S. TOMARU, *Jpn. J. Appl. Phys.* **19**(11) (1980) 2047.
26. N. P. BANSAL and R. H. DOREMUS, "Handbook of glass properties" (Academic press, 1986) 25.
27. R. H. DOREMUS, "Glass Science" (Wiley, New York, 1973) 121.
28. A. M. EFIMOV, *J. Non-Cryst. Solids* **203** (1996) 1.

Received 11 November 1998
and accepted 18 May 1999